FOURTH SEMIANUAL PROGRESS REPORT

TO: NATIONAL AERONAUTICS AND SPACE ADMINISTRATION
AMES RESEARCH CENTER

P. 34

FROM: NORTH CAROLINA STATE UNIVERSITY, RALEIGH, NC 27695

FOR: "HETEROGENEOUS PHOTOCATALYTIC OXIDATION OF ATMOSPHERIC TRACE CONTAMINANTS"
NASA RESEARCH GRANT 2-684

BY: DAVID F OLLIS
CHEMICAL ENGINEERING DEPARTMENT
NORTH CAROLINA STATE UNIVERSITY
RALEIGH, NC 27695
PHONE: (919)-515-2329
FAX (919)-515-3465

PERIOD COVERED: 5/1/92-10/31/92

PRINCIPAL INVESTIGATOR: DAVID F. OLLIS

SUBMITTED: 4/2/93 (PRELIMINARY VERSION JANUARY, 1993)

TABLE OF CONTENTS

REPORT

REPORT

1. Photoreactor monolith fundamental studies (Y. LUO)

(a) Monolith reactor models

Catalytic monoliths have a good prior history in automobile exhaust control for emission reduction of carbon monoxide and unburned hydrocarbons. Prior reactor modeling of this catalytic configuration operating in a thermal (rather than the present photochemical) mode has included either fully developed flow patterns or plug flow (flat) velocity patterns. The major exception to this claim is the work of Boersma et al (1987) who included the more difficult analysis involving the development of the full velocity field from the entrance condition of a flat or plug flow velocity profile. Long channel monoliths can utilize the fully developed flow approximation, since the (nearly) parabolic developed flow profile is achieved early in such a channel system. Our photocatalytic monolith will use a channel length of six inches (commercial auto exhaust configuration) or shorter (to allow for more internal illumination) We evaluate this entrance problem below.

(b) Entrance length effects

The velocity model required depends on the fraction given by the ratio of the entrance distance required for parabolic flow development divided by the full channel length. A small fraction means that almost the entire channel operates under developed flow; a ratio closer to unity means the opposite.

The criteria for estimating the entrance lengths for the velocity and concentration fields depend on the Reynolds number (Re) and the Schmidt number (Sc).

For velocity, the entrance length in terms of monolith channel diameter, d, is given by

1

$Z/d = 0.06\ Re$

For concentration fields, the entrance length is given by

$Z/d = 0.06\ Re\ Sc$

For gases, the Schmidt number is unity, thus the entrance lengths for development of both concentration and velocity fields is the same.

As the range of Reynolds numbers examined is between 10 and 150, the velocity entrance length is 0.6 up to 9.0 channel diameters, coreesponding to 2% up to 30 % of the channel length. Because the illumination field will actually be non-uniform, and most intense near the entrance , we expect that a full entrance flow analysis is required, since the entrance criteria defined above are from literature sources which assume a uniform wall activity, whereas the non-uniform photocatalyst wall activity will be strongest in the developing flow entrance region.

(c) Gas flow velocity field

The velocity flow field is summarized in Table 1. The model assumptions include steady state, incompressible flow, Newtonian fliuid, axisymmetric velocity profile, and a uniform velocity profile upstream of the monolith channel entrance.

(d) Gas concentration field

The concentration field equations for the same problem are summarized in Table 2. This is a full analysis, including both axial and radial dispersion of the contaminant(s) in the gas phase flow. The need for axial dispersion, neglected in most previous monolith analyses, will be shown in the results section.

(e) Illumination: uniform vs. non-uniform

Model calculations were carried out for two circumstances: uniform wall intensity and non-uniform intensity, corresponding

respectively to uniform and non-uniform wall photocatalyst rate constants.

(f)   Results: acetone, 1-butanol design calculations

Using the photocatalytic rate constants for acetone and 1-butanol conversion reported earlier in this grant by Peral and Ollis (1992), we calculated concentration profiles for acetone and butanol as a function of axial position along the monolith (length = 30 channel diameters , i e., d = 0.4 cm and L = 30 x 0.4 = 12 cm or about 5 inches.

Acetone conversion profiles (Figure 2) indicate a nearly linear pattern at all Reynolds numbers (flow rates), consistent with the expectation that for a feed concentyration of 712.5 mg/m^3 (SMAC level), the reaction kinetics are zero order in acetone (Peral and Ollis(1992)).   Conversion varied between about 5% per pass at Re = 150 to about 65% per pass at Re = 10.

Lower acetone feed concentrations exhibit the curvature expected of positive order kinetics (Figure 3; examine curve for feed = 0.1 SMAC or 71.2 mg/m^3)

Butanol conversion profiles are strongly curved, again as expected since the conversion kinetics are nearly first order in 1-butanol at the SMAC levell assumed of 121. mg/m3.(Peral and Ollis(1992).

The same variations of butanol feed concentrations produces   the same
$C(z)/C_0$ curve, reflective of the essentially first order variation of rate with concentration at all concnetrations under consideration (Figure 4)

(g)   Mass transfer influence

The computed centerline, mixing cup averaged, and wall concentration profile for acetone (Figure 5a) shows very little

3

difference . This result indicates a nearly uniform radial concentration profile for acetone, i.e, radial mass transfer rates are sufficient and the overalll rate is limited by the photocatalyst wall kinetics.

For the more reactive 1-butanol, however, the same calculations (Fig 5b) indicate that substantial differences of 10-30 % between centerline and wall concentrations may exist at any point in the channel. This results means the mass transfer resistances are appreciable and the presumed requirement for radial mass transfer by convective diffusion using a second order radial term is verified (Table 2).

(h) Non-uniform illumination influence

Calculations assuming an illumination decrease varying inversely with distance between the lamp and channel wall are summarized in Figures 6a (acetone) and 6b (1-butanol). A point source lamp is positioned at 1, or 10, or 50 channel diameters upstream of the monolith (corresponding to 0.4 cm, 4. cm and 20 cm., respectively) For acetone, the corresponding conversion per pass for a point source lamp changes from 100 % to 35 % to 1 % (Figure 6a). For butanol, the corresponding conversions are 100 %, 100 % and 25 % (Figure 6b)

These calculations indicate that for a point source lamp , the variation of rate with lamp position is very important. A fuller calculation using a more realistic planar light source approximation for our lamps is underway and will be reported at a later time in this study.

(i) Conclusions

The first photocatalytic monolith model has been constructed and used to predict concentration profiles for a weakly reactive (acetone) and a moderately reactive (butanol) pollutant for various conditions of flow (Reynolds number), entrance concentrations, and illumination fields. The model appears robust, and we will improve it by inclusion of more realistic illumination fields and by

confrontation withmeasured illumination and axial concentration fields later in this study.

2. Monolith reactor operation: batch recirculation system   (M. Sauer)

(a)   Expermmental set-up

A recirculating monolith reactor, analogous to that published by Suzuki et al of Toyota Laboratories (1991) was constructed of transparent plexiglas tubes; a schematic appears in Figure 7. the reactor consists of 6 " diameter tubing, two 100 watt near UV ("black") lights, a variable speed recirculation fan (to allow various Reynolds number operations) and a sample injection and withdrawal port.

(b)   Results

(i)   Acetone adsorption

All application of photocatalysis to air purification and treatment is likely to involved humidified air. As both acetone and water adsorb on the monolith support as well as the photocatalyst titanium dioxide phase, and as the support mass is far larger than that of the catalyst 10 μm coating, the adsorption isotherms on the support need determination. Figure 8 presents the variation of acetone mass adsorbed as a function of gas phase concentration of acetone at five different injected water contents. (The relative humidities were not measurable at this time; an equipment modification is underway to measure relative humidity and contaminant levels simultaneously)   This figure shows the importance of relative humidity in influencing the acetone partitioning between the gas phase and monolith surface .   Our reactor models   includes this influence explicity.

(ii) Acetone kinetics

Batch experiments in the recirculating apparatus of Figure 8 were accomplished at initial concentrations between 100 and 700 mg/m^3 acetone. Initial rate analysis indicated that the data could be fitted to a Langmuir Hinshelwood model, as indicated by the linearity of a plot of inverse initial rate vs inverse initial concentration (Figure 9) (lowest concentration point ignored, as this point was our first run and is not considered particularly reliable)

(iii) Model development

The conversion per pass is several percent under appreciable flow rates in the recirculation system. Under this circumstance, the monolith reactor can be used as a test of kinetic forms over the entire course of a batch conversion, since the system as a whole behaves as a well stirred reactor. (Later experiments in spring and summer of 1993 will explore integral conversion operation at slower flow rates) Under this circumstance, we have developeed a kinetic model for the reactor system, summarized in Appendix A (pp A.1-A.4) The final equation contains only the independent variable , time, and the sole dependent variable, C(t). The kinetic model includes the following:

acetone and water adsorption on monolith

acetone photocatalyst reaction

system and catalyst volumes

water photocatalyst inhibition (from Peral et al (1992))

constant relative humidity (water of reaction small vs. water for humidification)

(iv) Comparison: model vs experiment

The data and model for five initial conditions are summarized in Figure 10a-e. The agreement is generally good, and we conclude that for acetone conversions, where no appreciable intermediates are detectable, the simple model in Appendix A is adequate for reactor design purposes.

Given the adequacy of the model here, it is also useful to consider the predicted influence of water vapor variation. Calculations to this end are presented in Figure 10. An improved version of this model will be developed in spring -sumer of 1993 when we are able to determine the water adsorption isotherm experimentally and incorporate this more realistic function for the humidification influence on both the monolith and the catalyst.

(v) Dual reactant experiments

Two runs have been performed to date using dual reactant feed. Figure 12a indicates that m-xylene, an aromatic, is converted more rapidly than acetonein a two component acetone-xylene feed. This result is expected as unsaturates have intermediate to high reactivity vs saurated oxygenates. Figure 12b compares the acetone vs time concentration profiles for acetone only (triangles) and acetone with m-xylene (open squares). This figure indicates that a clear competitive inhibition exists when multiple reactants are converted simultaneously. This competitive inhibition is found to occur also with all other forms of catalysis where a large number of reactant molecules compete for a limited number of catalyst sites. The next year will include development of two and three component contaminant models and confrontation with data such as that of Figures 12a and 12b.

7

Table 1

II. Problem formulation

Entrance velocity field

Model assumptions
  (1). Steady state
  (2). Incompressible flow
  (3). Newtonian fluid
  (4). Axisymmetrical velocity profile
  (5). Uniform velocity profile before tube entrance

The dimensionless forms of the governing equations are:

$$V\frac{\partial v}{\partial r} + U\frac{\partial V}{\partial Z} = -\frac{1}{U_m^2\rho}\frac{\partial P}{\partial r} + \frac{2}{Re}\left(\frac{\partial^2 V}{\partial r^2} + \frac{1}{r}\frac{\partial V}{\partial r} - \frac{V}{r^2} + \frac{\partial^2 V}{\partial Z^2}\right)$$

$$V\frac{\partial U}{\partial r} + U\frac{\partial U}{\partial Z} = -\frac{1}{U_m^2\rho}\frac{\partial P}{\partial Z} + \frac{2}{Re}\left(\frac{\partial^2 U}{\partial r^2} + \frac{1}{r}\frac{\partial U}{\partial r} + \frac{\partial^2 U}{\partial Z^2}\right)$$

$$\frac{\partial V}{\partial r} + \frac{V}{r} + \frac{\partial U}{\partial Z} = 0$$

Define stream function and vorticity function as following:

$$U = -\frac{1}{r}\frac{\partial\Psi}{\partial r}$$

$$V = \frac{1}{r}\frac{\partial\Psi}{\partial Z}$$

Table 1 (cont'd)

The only non zero component of the vorticity vector is the azimuthal component, which is given by:

$$\omega = \frac{\partial V}{\partial Z} - \frac{\partial U}{\partial r}$$

The equations we need to solve become:

$$-\frac{\omega}{r^2}\frac{\partial \psi}{\partial Z} + \frac{1}{r}\frac{\partial \psi}{\partial Z}\frac{\partial \omega}{\partial r} - \frac{1}{r}\frac{\partial \psi}{\partial r}\frac{\partial \omega}{\partial Z} =$$

$$\frac{2}{Re}\left(\frac{\partial^2 \omega}{\partial r^2} + \frac{1}{r}\frac{\partial \omega}{\partial r} - \frac{\omega}{r^2} + \frac{\partial^2 \omega}{\partial Z^2}\right)$$

$$\omega r = \left(\frac{\partial^2 \psi}{\partial r^2} - \frac{1}{r}\frac{\partial \psi}{\partial r} + \frac{\partial^2 \psi}{\partial Z^2}\right)$$

The boundary conditions are:

$$Z=0,\ 0\leq r\leq 0.5,\ \omega=0,\ \psi=-0.5r^2$$
$$Z>0,\ r=0,\ V=\omega=0,\ \psi=0$$
$$Z>0,\ r=0.5,\ \omega= 2\frac{\partial^2 \psi}{\partial r^2},\ \psi=-0.125$$
$$Z=30.0,\ 0\leq r\leq 0.5, \frac{\partial \omega}{\partial Z} = 0,\ \frac{\partial \psi}{\partial Z} = 0$$

Table 2

Entrance concentration field

Surface reaction on the catalyst wall

The dimensionless governing equation for concentration profile in the single channel of monolith reactor is:

$$\frac{\partial^2 C}{\partial r^2} + \frac{1}{r}\frac{\partial C}{\partial r} + \frac{\partial^2 C}{\partial Z^2} = \frac{Pe}{2}\frac{\partial UC}{\partial Z} + \frac{Pe}{2r}\frac{\partial(rVC)}{\partial r}$$

The boundary conditions are:

$$z>0, \ r=0, \ \frac{\partial C}{\partial r} = 0$$

$$z=0, \ 0\leq r \leq 0.5, \ C=1$$

$$z>0, \ r=0.5, \ \frac{\partial C}{\partial r} = -Da\,\frac{KC}{1+KC}, \ \ Da=\frac{kd}{D_{AB}C_0}$$

$$z=30.0 \ (\text{exit}), \ 0\leq r \leq 0.5, \ \frac{\partial C}{\partial Z} = 0$$

III. Reactor analysis for pollutant conversions

- *Constant light intensity*

- *Point source light intensity*
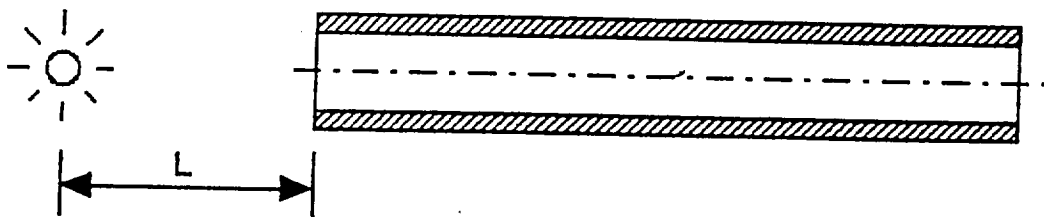
Figure 1
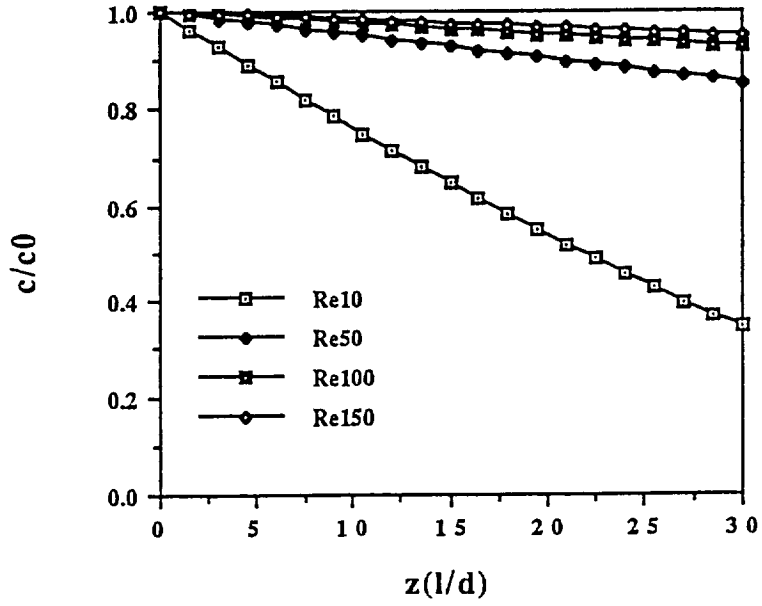
Computed acetone concentration profiles for Re=10, 50, 100, 150.
($c0=712.5$ mg/m^3, d=0.4 cm)

Figure 2a
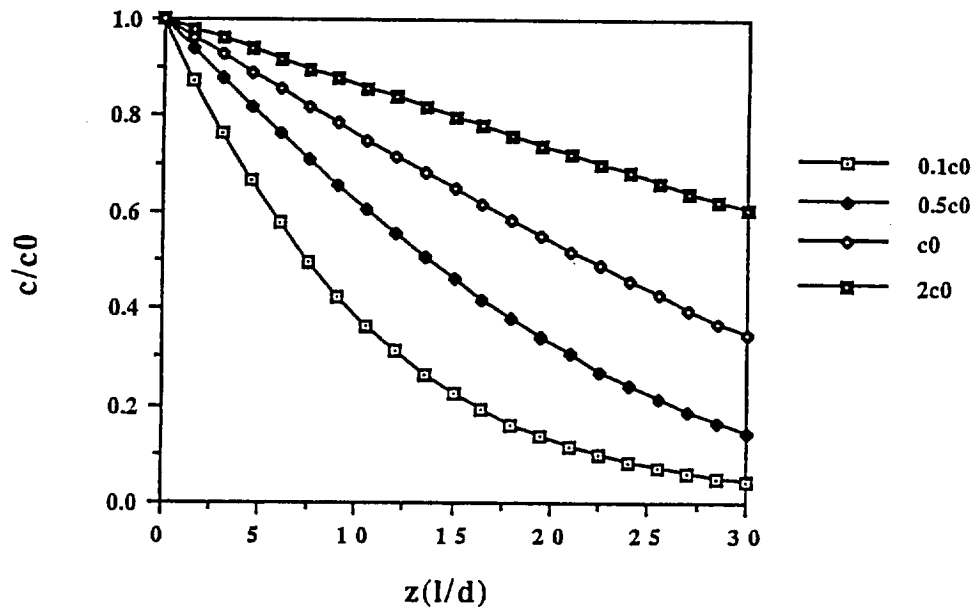
Computed profiles for various initial acetone concentrations

(Re=10, c0=712.5 mg/m^3, d=0.4 cm)

Figure 2b
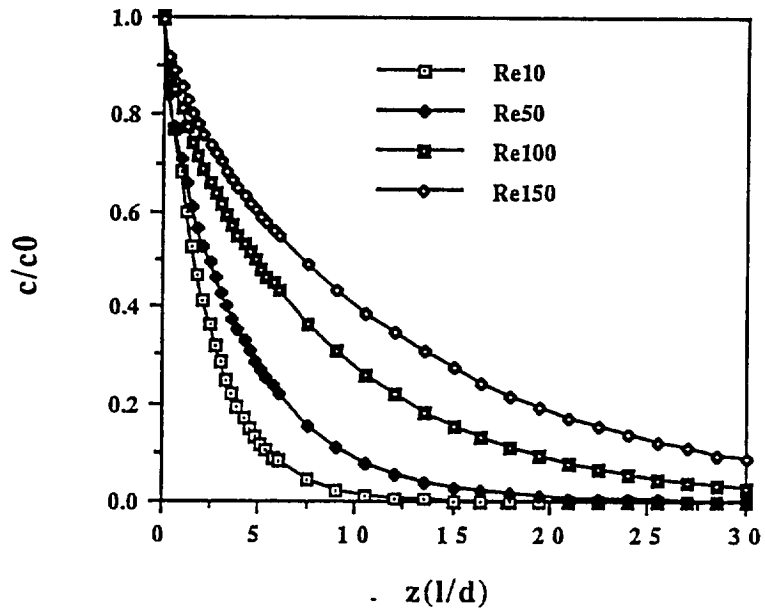
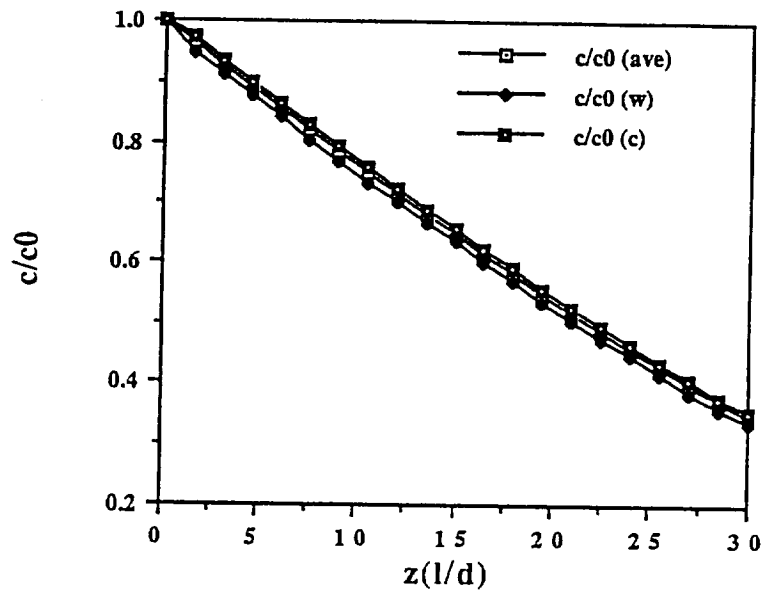Computed 1-butanol concentration profiles for Re10, 50, 100, 150.
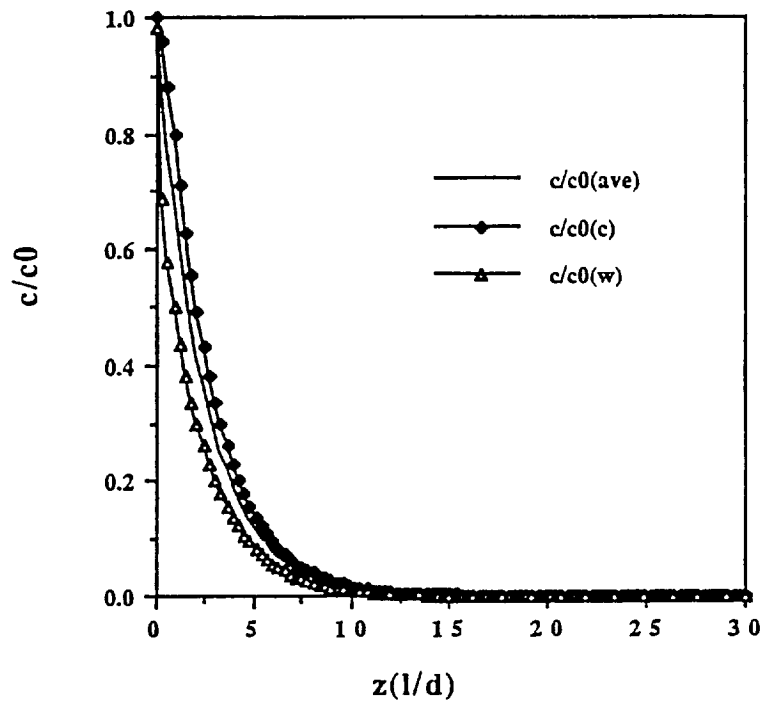
($c0=121.0$ mg/m^3, d=0.4 cm)

Figure 3
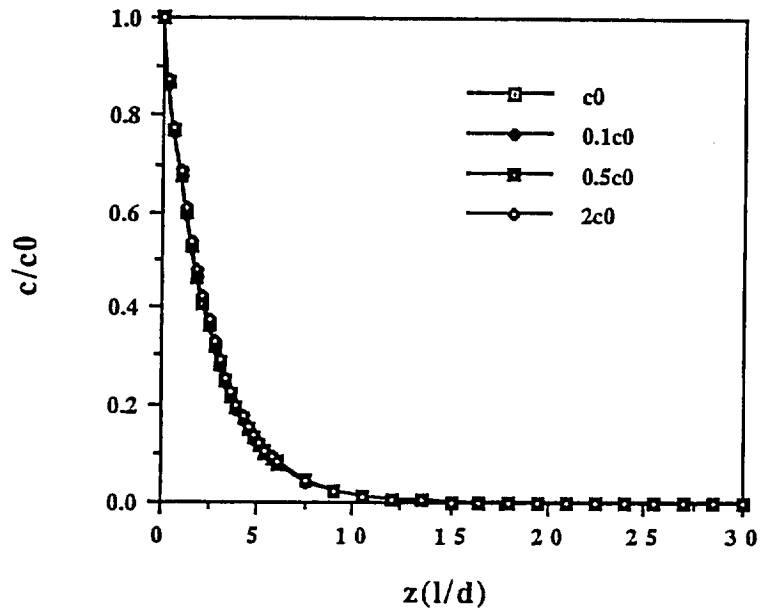
Computed profiles for various initial 1-butanol concentrations

(Re=10, c0=121.0 mg/m^3, d=0.4 cm)

Figure 4

Computed acetone wall, centerline, and average concentrations

(Re=10, c0=712.5 mg/m^3, d=0.4 cm)

Figure 5a

Computed 1-butanol wall, centerline, and average concentrations
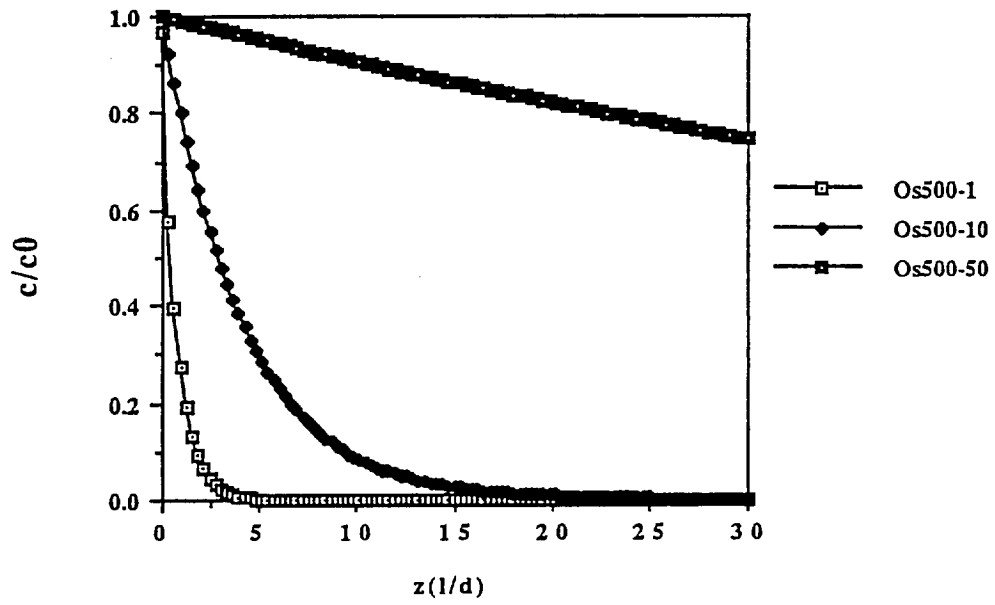
(Re=10, c0=121.0 mg/m^3, d=0.4 cm)

Figure 5b
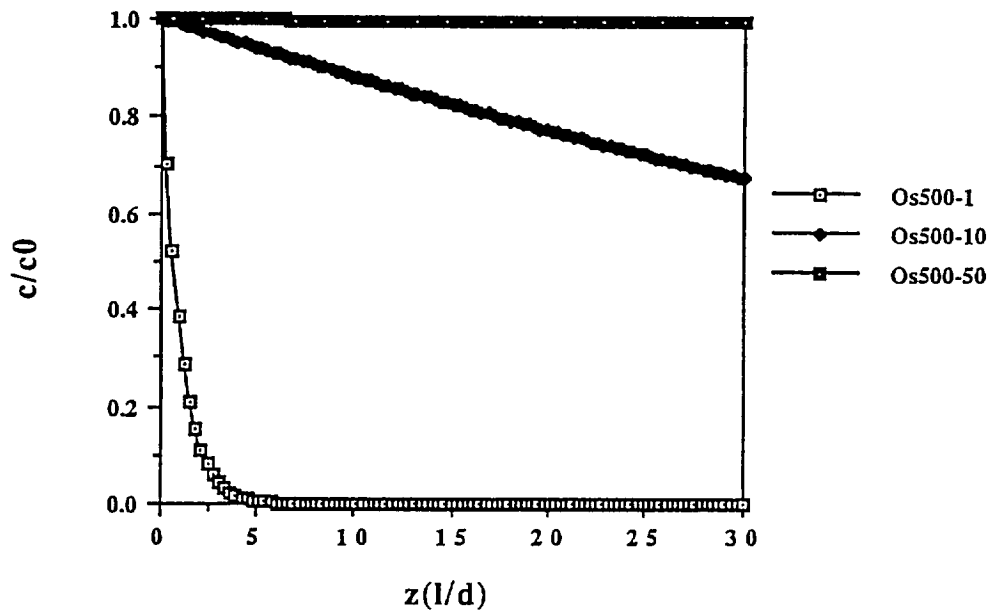
Acetone concentration profiles

(c0=712.5 mg/m^3, d=0.4cm, Osram HBO 500W point source lamp)

Figure 6a

c/c0

1.0

0.8

0.6

0.4

0.2

0.0

0   5   1 0   1 5   2 0   2 5   3 0

z(l/d)

Os500-1
Os500-10
Os500-50

1-Butanol concentration profiles

(c0=121.0 mg/m³, d=0.4cm, Osram HBO 500W point source lamp)

Figure 6b

19

• Experimental monolith reactor system setup

Figure 7

20
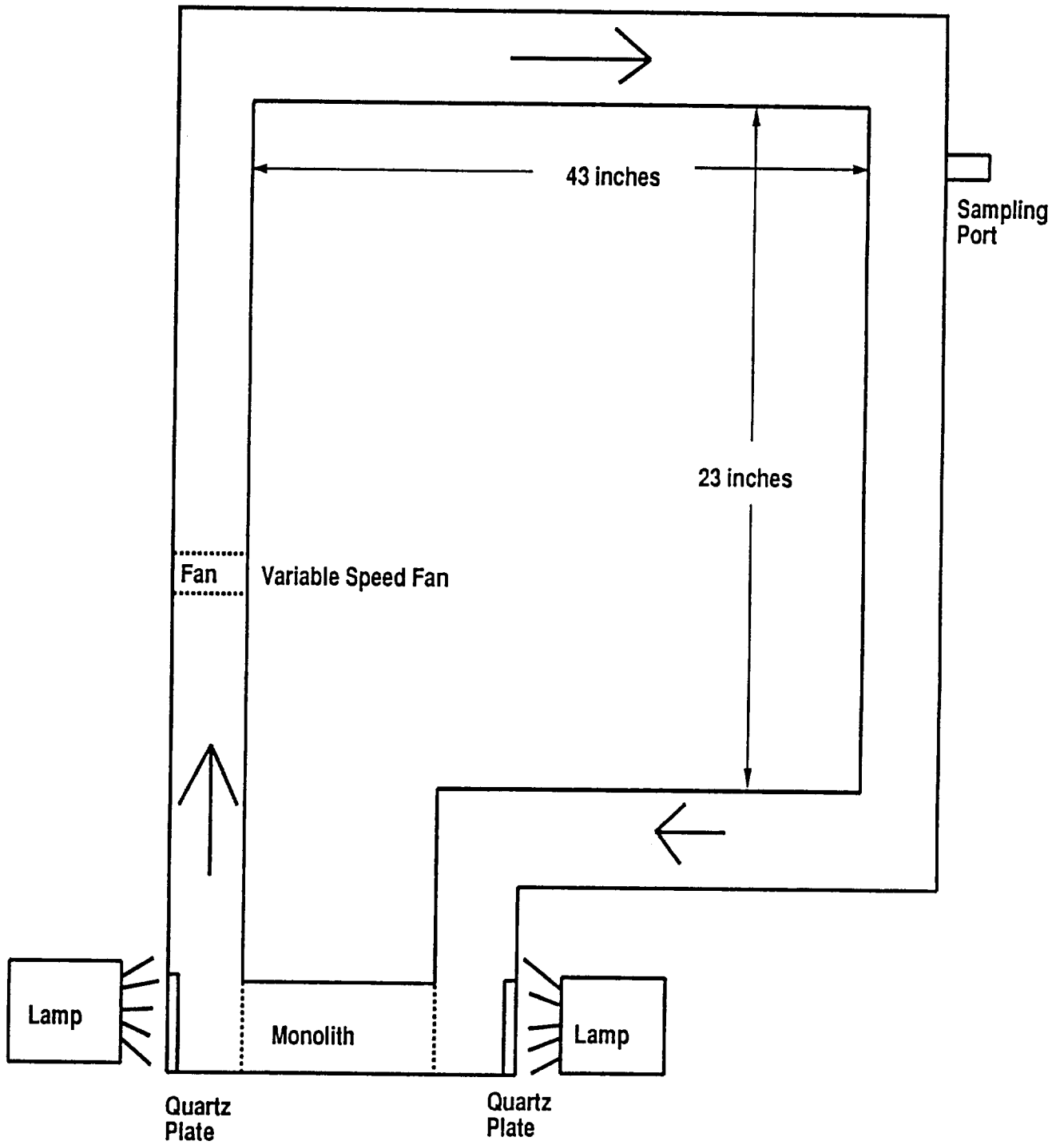
Acetone adsorption

- Mass of acetone adsorbed on monolith (M_A) verses steady state acetone gas phase concentration (C_A)
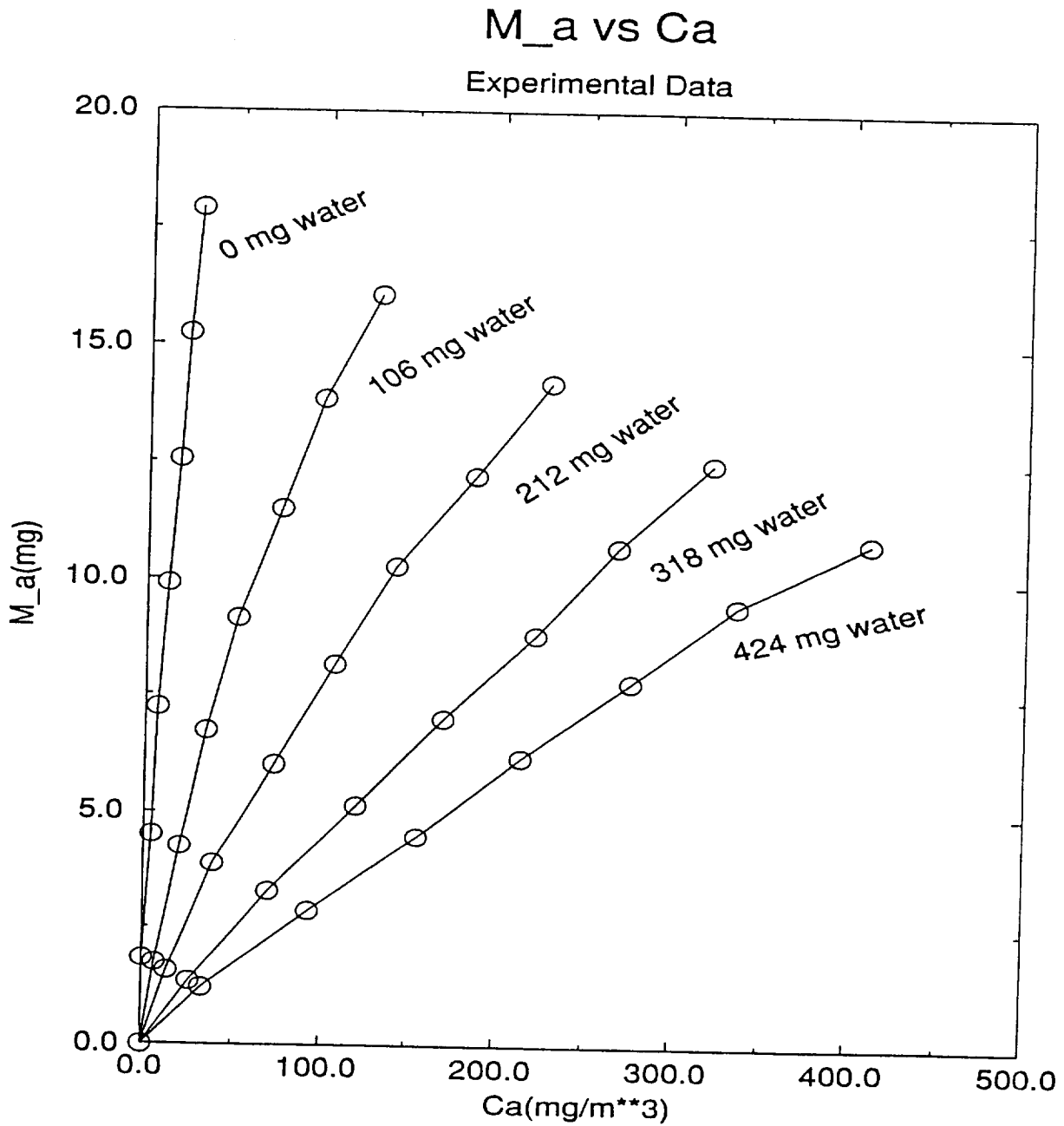

Figure 8

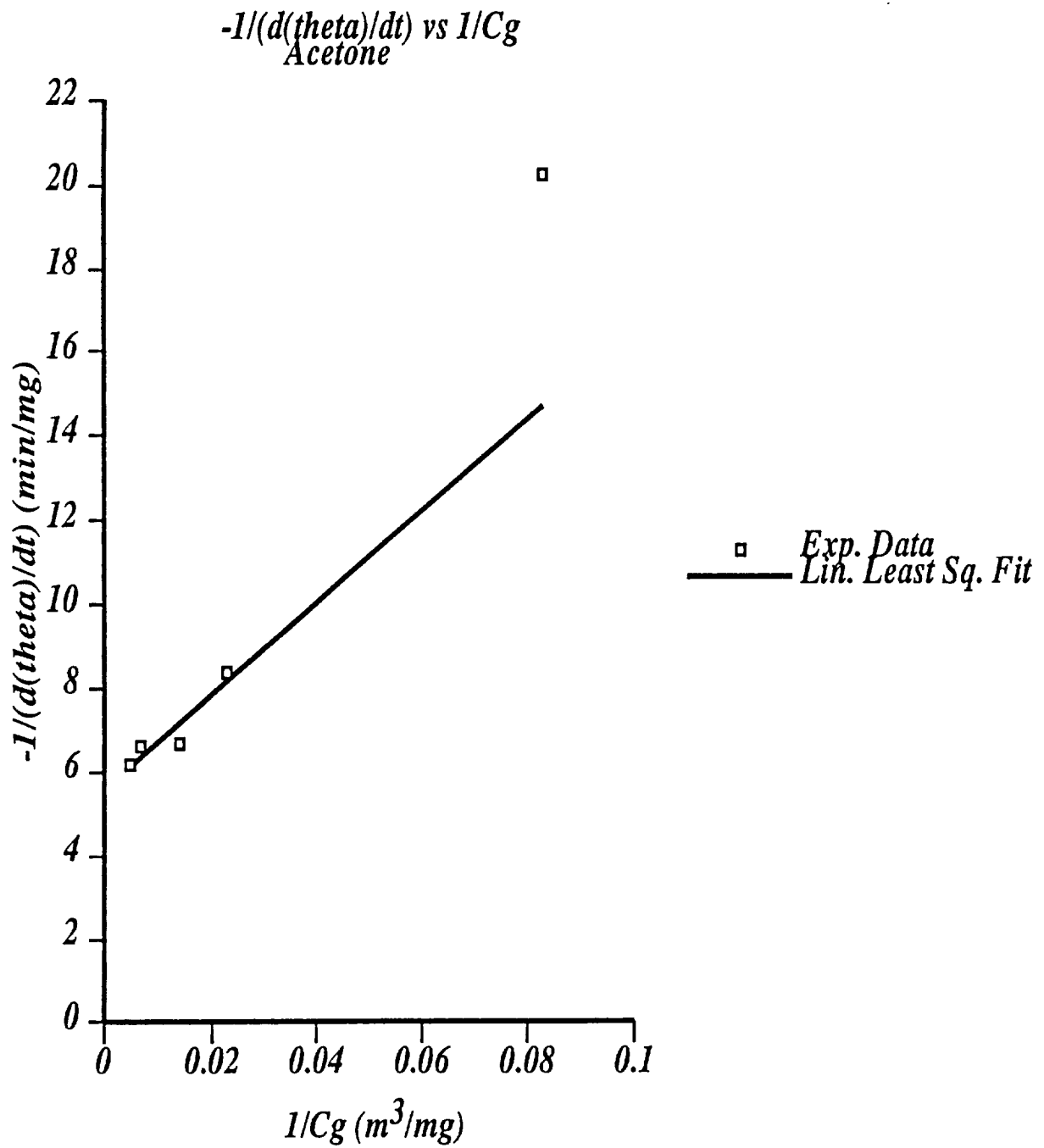- Determination of acetone kinetic parameters for axial flow monolith system

-1/(d(theta)/dt) vs 1/Cg
Acetone

Legend:
□ Exp. Data
— Lin. Least Sq. Fit

x-axis: 1/Cg (m³/mg)
y-axis: -1/(d(theta)/dt) (min/mg)

Figure 9

22

Model/Experiment comparison

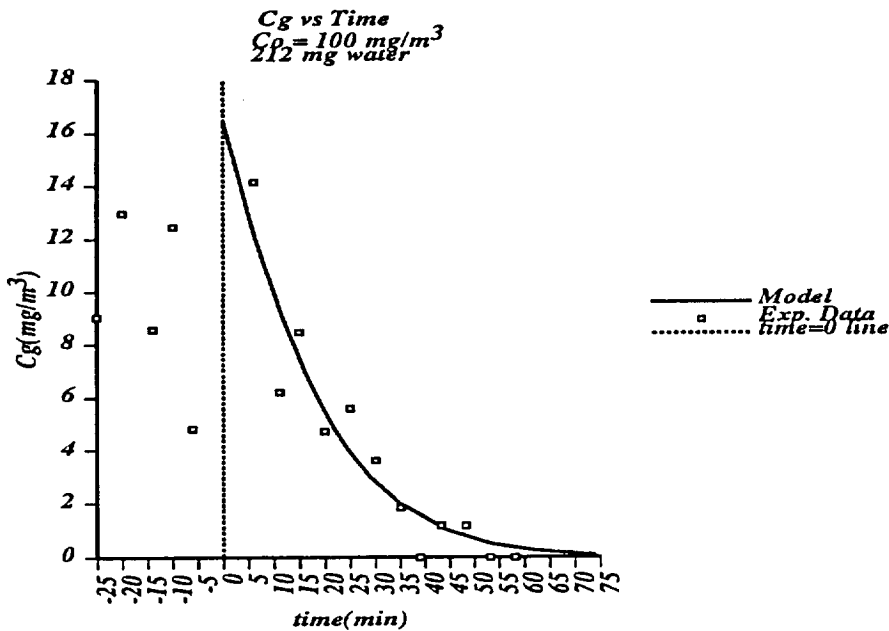- Model prediction for $C_0 = 100\frac{mg}{m^3}$ experimental data

Figure 10a

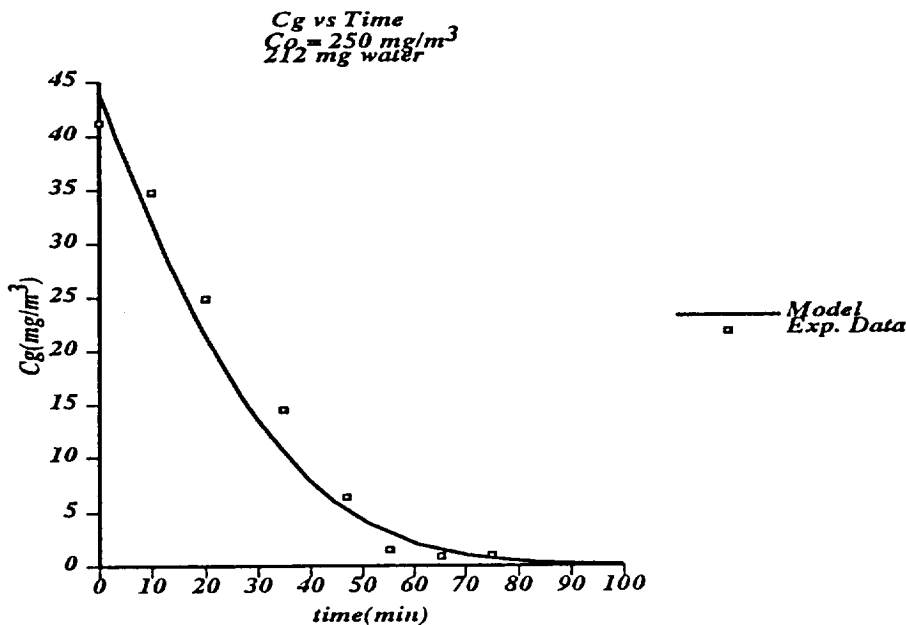- Model prediction for $C_0 = 250\frac{mg}{m^3}$ experimental data

Figure 10b

23

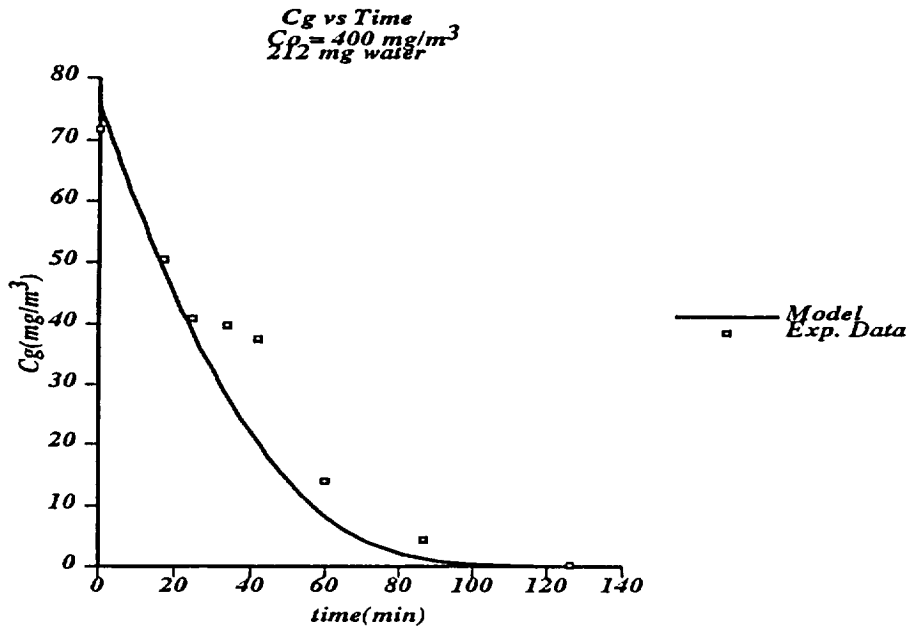- Model prediction for $C_0 = 400\frac{mg}{m^3}$ experimental data

Figure 10c

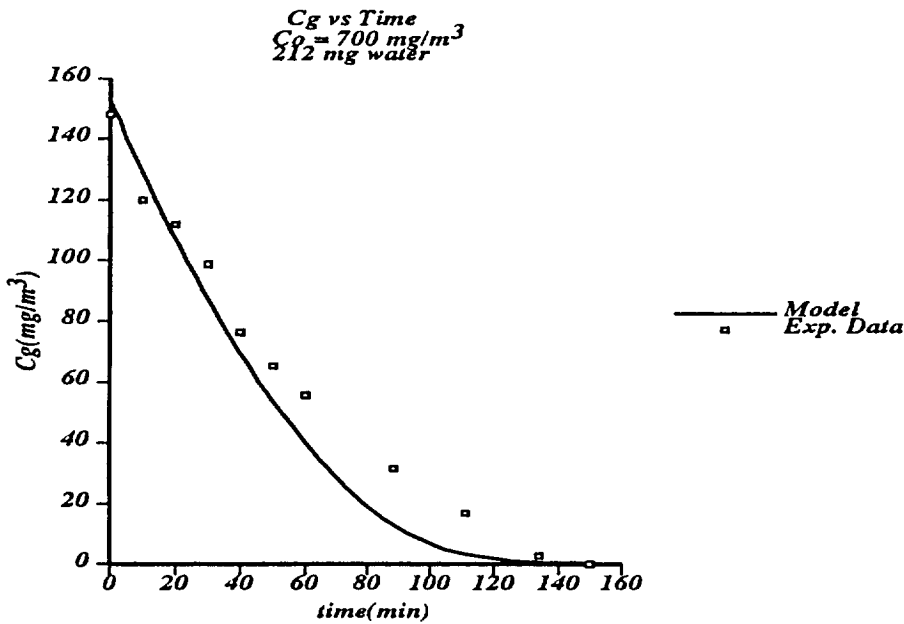- Model prediction for $C_0 = 700\frac{mg}{m^3}$ experimental data

Figure 10d

24

- Model prediction for $C_0 = 1000\frac{mg}{m^3}$ experimental data
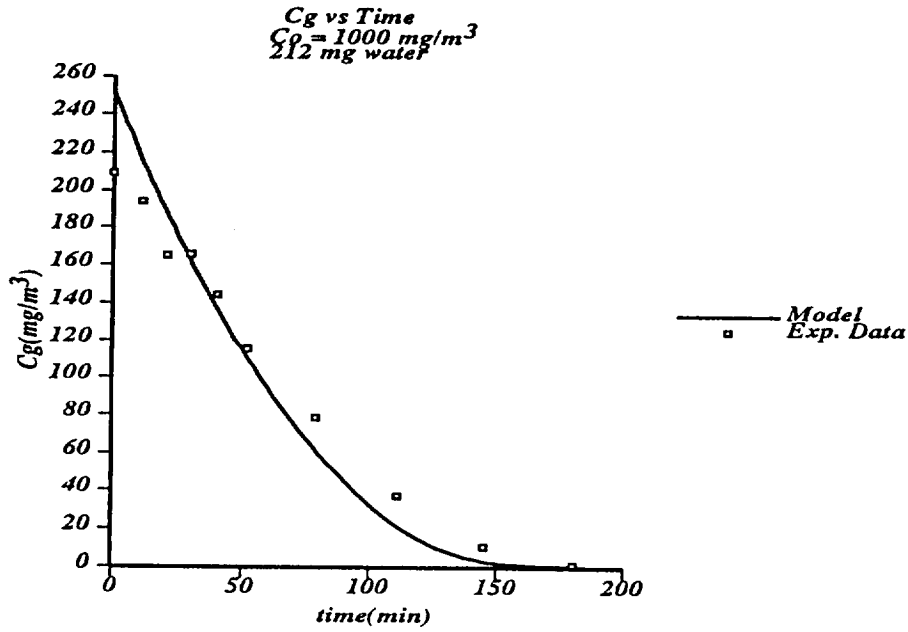

Figure 10e

- Short time model prediction of water inhibition effect

Cg vs Time
Co = 400 mg/m³
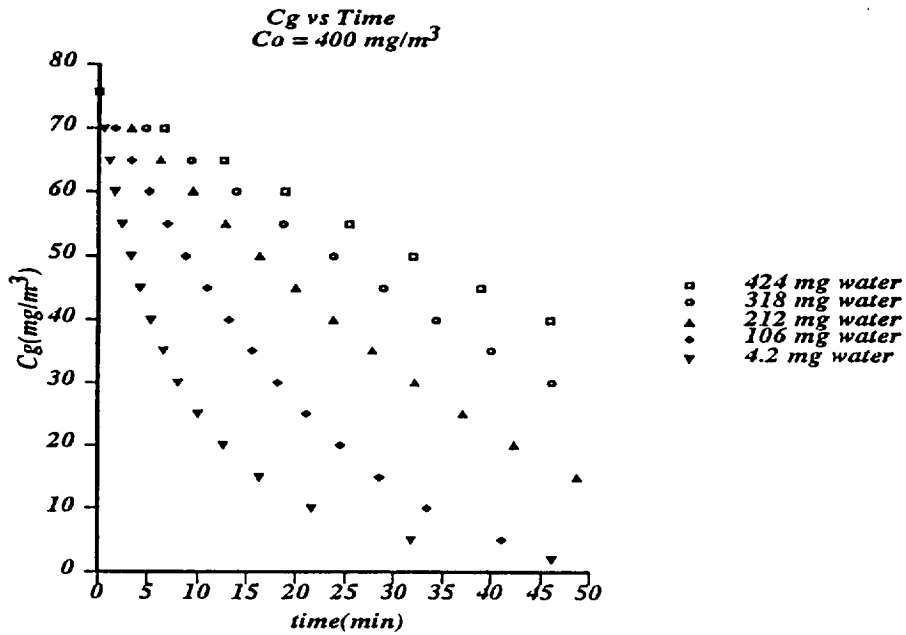
Figure 11a

- Long time model prediction of water inhibition effect

Cg vs Time
Co = 400 mg/m³

Figure 11b

26
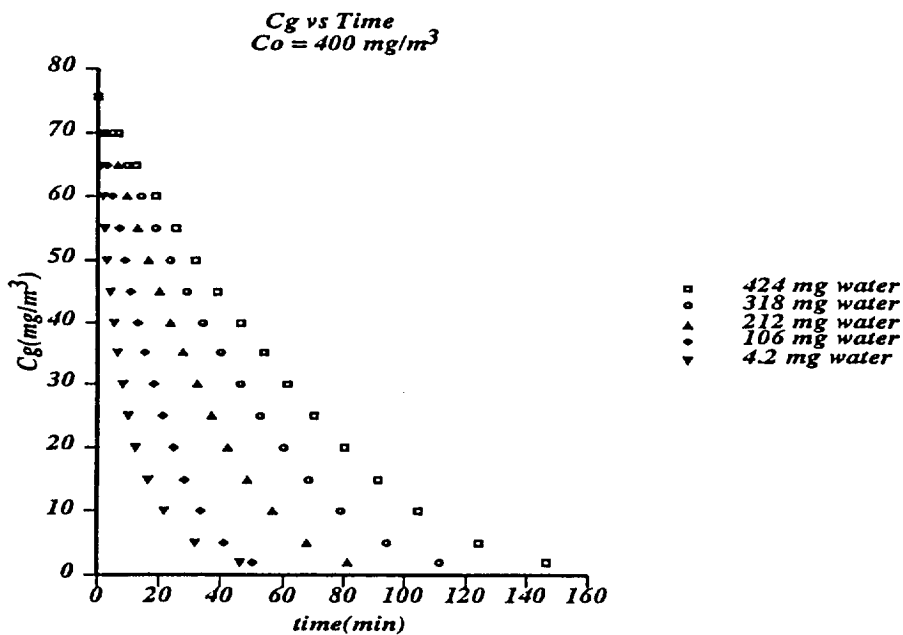
Two reactant experiment

- Acetone/m-Xylene mixed feed experimental result

Concentration vs Time
Acetone/m-Xylene
$C\rho = 400\ mg/m^3$
212 mg water
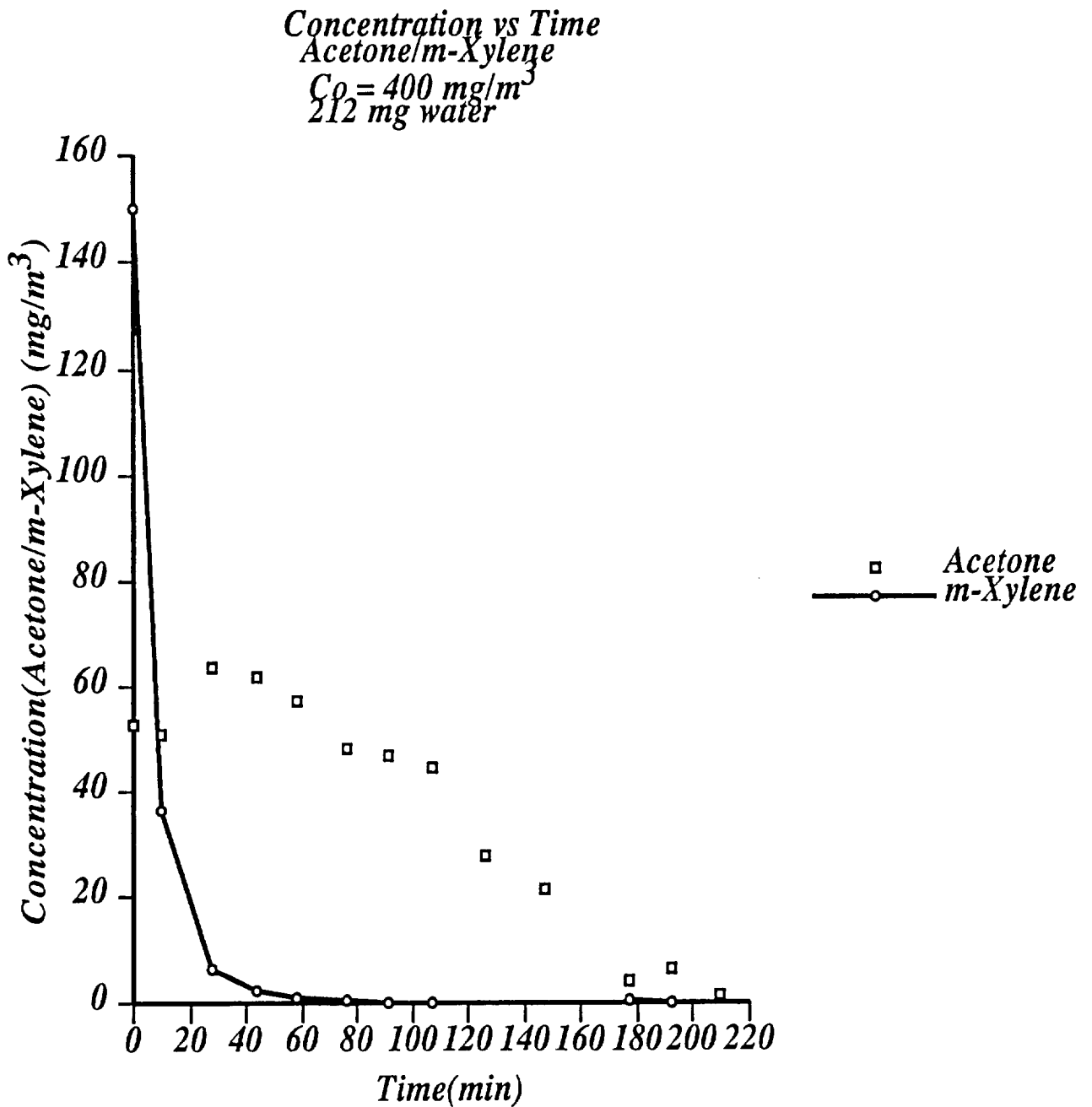
Figure 12a

- Comparison of Acetone Single Feed and Mixed Feed Runs

Concentration vs Time
Acetone
$C_0 = 400 \ mg/m^3$
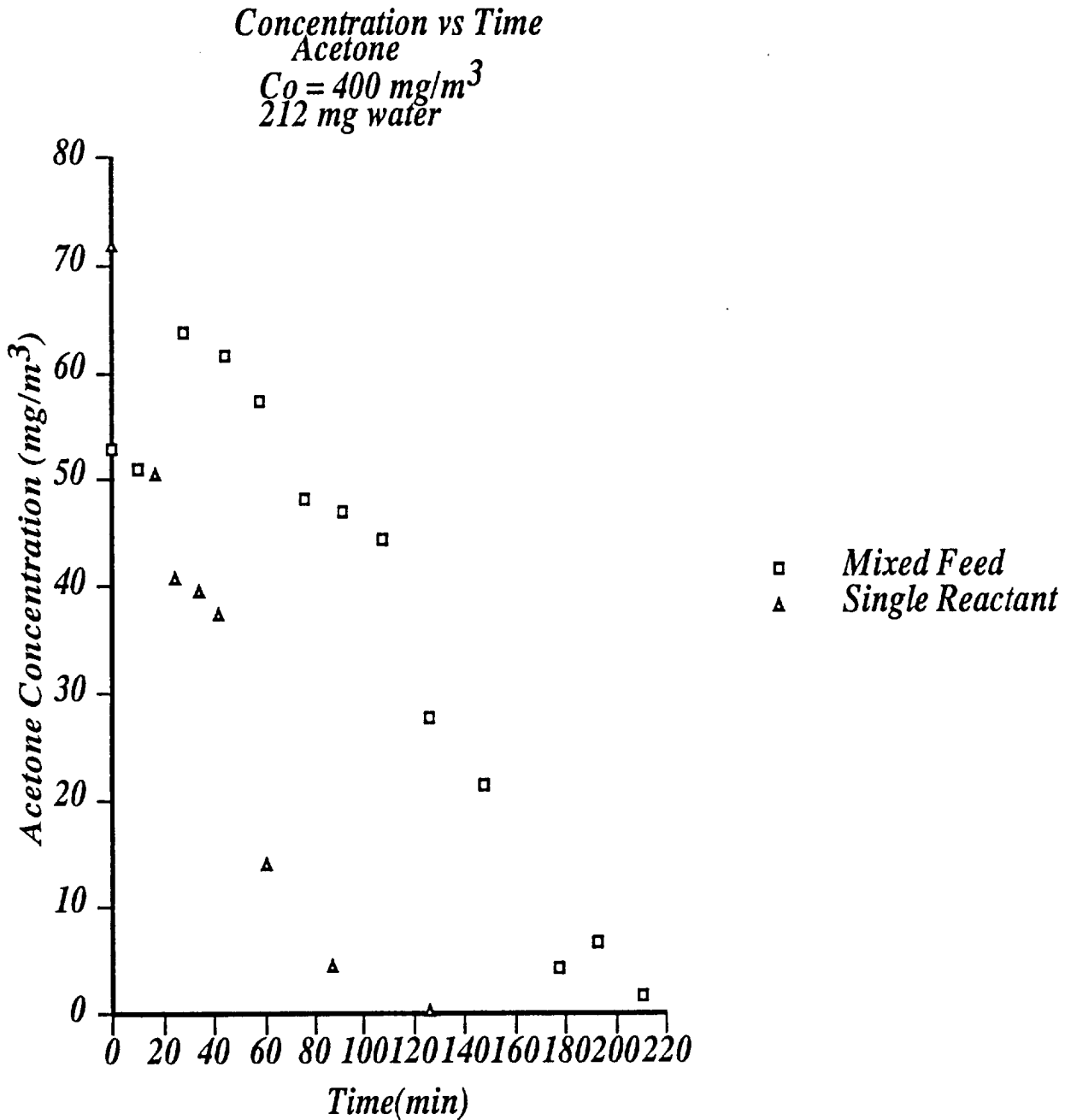$212 \ mg \ water$

□ *Mixed Feed*
▲ *Single Reactant*

Figure 12b

28

Model development

♣A reactant species mass balance assuming the recycle loop is plug flow (PF),

$$\frac{d}{dt}\left(\int_0^L C_s(z)dz\right) = \frac{q(C_2 - C_1)}{A_s} \tag{1}$$

Assumptions(PF):

- Plug flow

- No reaction occuring

- Isothermal

If we assume a well mixed recycle loop, (i. e. $C_s \neq f(z)$), with $A_s L = V_s$,

$$V_s \frac{dC_s}{dt} = q(C_2 - C_1) \tag{2}$$

Equation 2 is the equation for a CST, with $C_s \equiv C_1$

♣A reactant species mass balance on the CSTR gives,

$$q(C_1 - C_2) - \frac{kKC_R V_c^{act}}{1 + KC_R} = V_R \frac{dC_R}{dt} + \frac{dM_R}{dt} \tag{3}$$

Assumptions(CSTR):

- Neglect mass transfer effects

- Reaction follows a simple LH rate form

- Well mixed system

- $C_R \approx \frac{C_1 + C_2}{2} = \overline{C}$

- Isothermal

Combining Equations 2 and 3,

$$-\frac{kKC_R V_c^{act}}{1+KC_R} = \left(V_R\frac{dC_R}{dt} + V_s\frac{dC_s}{dt}\right) + \frac{dM_R}{dt} \tag{4}$$

$$V_s + V_R = V_g \tag{5}$$

The conversion per pass for $C_0 = 100\frac{mg}{m^3}$ is $\approx 0.45\%$. For a low per pass conversion assume $(C_R \approx C_s) \equiv C_g$. This assumption also gives,

$$V_g\frac{dC_g}{dt} = V_R\frac{dC_R}{dt} + V_s\frac{dC_s}{dt} \tag{6}$$

Combining Equations 4 and 6,

$$-\frac{kKC_g V_c^{act}}{1+KC_g} = V_g\frac{dC_g}{dt} + \frac{dM_R}{dt} \tag{7}$$

Equation 7 has no fit parameters. Substituting the Langmuir isotherm for acetone,

$$-\frac{kKC_g V_c^{act}}{1+KC_g} = V_g\frac{dC_g}{dt} + \frac{d}{dt}\left(\frac{\mu_A K_A C_g}{1+K_A C_g + K_w C_w}\right) \tag{8}$$

The differentiation $\frac{d}{dt}\left(\frac{\mu_A K_A C_g}{1+K_A C_g+K_w C_w}\right)$ gives (assuming $C_w = constant$),

$$\frac{d}{dt}\left(\frac{\mu_A K_A C_g}{1+K_A C_g + K_w C_w}\right) =$$
$$\left(\frac{\mu_A K_A}{1+K_A C_g + K_w C_w}\right.$$
$$\left.-\frac{\mu_A K_A^2 C_g}{(1+K_A C_g + K_w C_w)^2}\right)\frac{dC_g}{dt} \tag{9}$$

Substituting Equation 9 into Equation 8,

$$-\frac{kKC_g V_c^{act}}{1+KC_g} = \left(V_g + \frac{\mu_A K_A}{1+K_A C_g + K_w C_w} - \frac{\mu_A K_A^2 C_g}{(1+K_A C_g + K_w C_w)^2}\right)\frac{dC_g}{dt} \tag{10}$$

A.2

Rearranging Equation 10 and integrating,

$$\int_0^t kKV_c^{act}dt =$$

$$-\int_{C_g(0)}^{C_g(t)} \left(\frac{1}{C_g} + K\right) \left(V_g + \frac{\mu_A K_A}{1 + K_A C_g + K_w C_w}\right.$$

$$\left. - \frac{\mu_A K_A^2 C_g}{(1 + K_A C_g + K_w C_w)^2}\right) dC_g \quad (11)$$

Evaluation of the integrals (assuming $C_w = constant$),

$$kKV_c^{act}t =$$

$$\left(V_g + \frac{\mu_A K_A}{1 + K_w C_w}\right) \ln\left(\frac{C_g(0)}{C_g(t)}\right) + KV_g(C_g(0) - C_g(t))$$

$$- \left(\frac{\mu_A K_A}{1 + K_w C_w}\right) \ln\left(\frac{1 + K_A C_g(0) + K_w C_w}{1 + K_A C_g(t) + K_w C_w}\right)$$

$$-\mu_A K K_w C_w \left(\frac{1}{1 + K_A C_g(0) + K_w C_w} - \frac{1}{1 + K_A C_g(t) + K_w C_w}\right) \quad (12)$$

Separating the water inhibition effect from the reaction rate constant (k) leads to a reaction rate constant (k_0) that is independent of water effects.

$$k = \frac{k_0}{1 + K_{w_A} C_w^a} \quad (13)$$

The water inhibition expression for acetone and the values for K_{w_A} and a were obtained from Peral and Ollis, and were assumed to be applicable in the current study. The water inhibition effect will be examined with the monolith system in future experiments. Substituting values for k, K_{w_A} and a into Equation 13 gives,

$$k_0 = 0.77\frac{mg}{cm^3 cat - min} \quad (14)$$

Where,

$$K_{w_A} = 9.6 \times 10^{-7}\frac{m^3}{mg}$$

$$a = 1.674$$

$$C_w = 11509\frac{mg}{m^3}$$

A.3

The resulting model equation is,

$$\frac{k_0 K V_c^{act}}{1 + K_{w_A} C_w^a} t =$$

$$\left(V_g + \frac{\mu_A K_A}{1 + K_w C_w}\right) \ln\left(\frac{C_g(0)}{C_g(t)}\right) + K V_g(C_g(0) - C_g(t))$$

$$- \left(\frac{\mu_A K_A}{1 + K_w C_w}\right) \ln\left(\frac{1 + K_A C_g(0) + K_w C_w}{1 + K_A C_g(t) + K_w C_w}\right)$$

$$- \mu_A K K_w C_w \left(\frac{1}{1 + K_A C_g(0) + K_w C_w} - \frac{1}{1 + K_A C_g(t) + K_w C_w}\right) \quad (15)$$

Equation 15 utilizes no fit parameters:

- Acetone adsorption Langmuir fit $\Longrightarrow \mu_A, K_A, K_w$

- Acetone kinetic parameters $\Longrightarrow k, K$

- System physical constants $\Longrightarrow V_c^{act}, V_g$

- Dr. Peral's water inhibition constants $\Longrightarrow K_{w_A}, a$

- Water independent reaction rate constant $\Longrightarrow k_0$

- Assume $C_w = $ constant, $C_g(0) = $ constant (initial gas phase acetone concentration)

A.4